Spectroscopy of ^{257}Rf

J. Qian,[1] A. Heinz,[1] T. L. Khoo,[2] R. V. F. Janssens,[2] D. Peterson,[2] D. Seweryniak,[2] I. Ahmad,[2] M. Asai,[3] B. B. Back,[2] M. P. Carpenter,[2] A. B. Garnsworthy,[1,4] J. P. Greene,[2] A. A. Hecht,[2,5] C. L. Jiang,[2] F. G. Kondev,[2] T. Lauritsen,[2] C. J. Lister,[2] A. Robinson,[2] G. Savard,[2] R. Scott,[2] R. Vondrasek,[2] X. Wang,[2] R. Winkler,[1] and S. Zhu[2]

[1]*WNSL, Yale University, New Haven, Connecticut 06511, USA*

[2]*Argonne National Laboratory, Illinois 60439, USA*

[3]*Japan Atomic Energy Agency, Tokai, Ibaraki 319-1195, Japan*

[4]*University of Surrey, Guildford, GU2 7XH, United Kingdom*

[5]*University of Maryland, College Park, Maryland 20742, USA*

(Received 21 March 2009; published 22 June 2009)

The isotope ^{257}Rf was produced in the fusion-evaporation reaction ^{208}Pb(^{50}Ti, n)^{257}Rf. Reaction products were separated and identified by mass. Delayed spectroscopy of ^{257}Rf and its decay products was performed. A partial decay scheme with configuration assignments is proposed based on α hindrance factors. The excitation energy of the $1/2^+[620]$ configuration in ^{253}No is proposed. The energy of this $1/2^+$ state in a series of $N = 151$ isotones increases with nuclear charge, reflecting an increase in the $N = 152$ gap. This gap is deduced to grow substantially from 850 to 1400 keV between $Z = 94$ and 102. An isomeric state in ^{257}Rf, with a half-life of 160^{+42}_{-31} μs, was discovered by detecting internal conversion electrons followed by α decay. It is interpreted as a three-quasiparticle high-K isomer. A second group of internal conversion electrons, with a half-life of $4.1^{+2.4}_{-1.3}$ s, followed by α decay, was also observed. These events might originate from the decay of excited states in ^{257}Lr, populated by electron-capture decay of ^{257}Rf. Fission of ^{257}Rf was unambiguously detected, with a branching ratio of $b_{\mathrm{Rf}}^{\mathrm{SF}} = 0.02 \pm 0.01$.

DOI: 10.1103/PhysRevC.79.064319 PACS number(s): 23.35.+g, 23.20.Nx, 21.10.Tg, 23.60.+e

I. INTRODUCTION

Finding and understanding the limits in mass and charge of the nuclear landscape is one of the fundamental goals of nuclear physics. With increasing proton number, the long-range Coulomb repulsion in heavy nuclei leads to a decrease in stability, and, according to the liquid-drop model, elements with proton number $Z \gtrsim 104$ should have vanishingly short spontaneous-fission half-lives. However, the observation (e.g., Refs. [1,2]) of superheavy nuclei with atomic numbers $Z \gtrsim 104$ indicates that these nuclei still have a sizable fission barrier. The latter owes its existence to the presence of shell gaps in the single-particle energies which lead to a barrier against fission despite the vanishing liquid-drop contribution. The last experimentally identified proton shell gap is at proton number $Z = 82$. For the next proton shell closure, a number of predictions exist, most prominently from microscopic-macroscopic and self-consistent nuclear mean-field models. The predictions for the proton gap differ quite substantially from $Z = 114$ [3], $Z = 120$ [4] to $Z = 126$ [5] and illustrate the need to test models with data from nuclei near the predicted shell closure(s).

The most basic predictions of nuclear structure models are the energies and configurations of states which can be compared with experimental data in the heaviest nuclei for which spectroscopic information is available. This approach led to significant results in Nobelium isotopes ($Z = 102$), indicating [6] that predictions based on a calculation with the "universal" Woods-Saxon potential are in this case in better agreement with experimental data than those obtained with the Skyrme Hartree-Fock-Bogoliubov (SHFB) [7] or relativistic mean-field (RMF) approaches [8]. The goal of the present work is to extend the limits of such tests to a larger atomic number by performing delayed spectroscopy of ^{257}Rf ($Z = 104$). Knowledge on excited states of this odd-even nucleus provides information on the single-particle energies of orbitals near the Fermi surface. The single-particle energies of isotopes with neutron number $N = 153$ are also interesting, because a deformed shell closure has been predicted theoretically at $N = 152$ [9,10] and has been confirmed experimentally [11,12].

From an experimental point of view, decreasing production cross sections of heavy nuclei, and, correspondingly, low event rates, complicate the proper identification of evaporation residues. However, the use of time- and position-correlated α-decay chains (e.g., Ref. [13]) allows an event-by-event identification in mass and charge. This approach cannot be applied if none of the elements of the decay chain can be linked to a known α decay, if the energies of different α decays are too close to resolve individual α lines, if the correlation times are too long, or if the decay occurs predominantly by spontaneous fission (e.g., Ref. [14]). The identification is further complicated by the fact that when nuclei are implanted in the detector, α transitions are distorted because of the summing of their energy signals with those of conversion and Auger electrons from coincident cascades. Moreover, not all α particles deposit their full energy in the detector. Therefore, additional experimental information is often important. In the present work, mass identification via the mass-to-charge-state resolving power of the Argonne Fragment Mass Analyzer provides such an additional parameter.

Low production cross sections also require the use of high beam intensities which may preclude the presence of γ-ray detectors around the target. The method employed in this work

is based on the observation of delayed radiation following isomeric or ground-state decay. Gamma-ray spectroscopy in high-Z nuclei is challenging, as electromagnetic transitions have a high probability of proceeding via conversion electrons. Identifying isomeric states and establishing their configurations is a first step toward delineating a level scheme under these difficult experimental conditions. In actinide and transactinide nuclei, high-K isomers have been identified (e.g., Refs. [6,15,16]). These isomers owe their existence to a large difference in the direction of the angular momentum vector between the isomeric level and lower lying states with respect to the symmetry axis of prolate-deformed nuclei. In ^{254}No, with $N = 152$, high-K isomers were found [6,16]. In particular, the presence of a $K^{\pi} = 8^{-}$ isomer in ^{254}No with a two-proton quasiparticle configuration suggests the possible occurrence of one or more high-K isomers with three-quasiparticle configurations in ^{257}Rf ($N = 153$) via the coupling of the two-proton pair with the unpaired neutron. This conjecture motivated in part the present measurements.

This work reports on a new study of ^{257}Rf. An isomeric state with a half-life of 160^{+42}_{-31} μs was discovered. In addition, possible evidence was also found for another long-lived state ($4.1^{+2.4}_{-1.3}$ s), but its origin could not be determined unambiguously. Events associated with spontaneous fission of ^{256,257}Rf were also observed. Note that the production cross section of ^{257}Rf, for the reaction used in this work, is below 50 nb [17,18].

II. EXPERIMENTAL DETAILS

A. Setup

The experiment was performed at Argonne National Laboratory, and ^{257}Rf was produced in the reaction ^{208}Pb(^{50}Ti, n)^{257}Rf. The ^{50}Ti beam was delivered by an electron cyclotron resonance (ECR) ion source and accelerated by the ATLAS (Argonne Tandem Linac Accelerator System) to a laboratory energy of 233 MeV. The isotopically enriched ^{208}Pb targets had a thickness of 0.5 mg/cm^2 with a 0.04 mg/cm^2 carbon backing on the upstream side of the target and a 0.01 mg/cm^2 carbon layer on the downstream side to prevent sputtering of the target material. The beam energy at the center of the target was 229.9 MeV (calculated with the code SRIM2008 [19]), and the average energy of the recoiling reaction products was 41.4 MeV upon exiting the target. The accumulated beam time for this measurement was 115 hours, with an average beam intensity of 115 pnA. To keep the targets from melting, 16 identical targets were mounted on a wheel with a radius of 15.5 cm [20]. The wheel rotated at a speed of 1800 rpm to distribute the beam-induced heat evenly among all targets. The beam was interrupted using a fast "sweeping" signal at wheel positions corresponding to the locations of the target frames. To further reduce the heat deposition in the targets, the beam spot was slightly defocused in the vertical direction from 0.5 to 1 mm by reducing the field in the last vertically focusing quadrupole before the target chamber. At the same time, vertical "wobbling" of the beam through current variation in a steering magnet was also applied and resulted in a beam spot of ∼5 mm (in the vertical direction). The charge state distribution of the recoiling evaporation residues (ERs) was reset by a 0.01 mg/cm^2-thick carbon foil mounted 38 mm downstream from the target [20]. Behind the target and the reset foil, the ERs were separated from nonreacting and scattered beam using the Argonne Fragment Mass Analyzer (FMA) [21]. The ERs were dispersed according to their mass-to-charge-state ratio (A/q) in the horizontal direction. Hence, the vertical wobbling of the beam did not affect significantly the A/q resolution of the spectrometer. Recoils with charge states of $q = 19$ and 20 were transported through the instrument. The setup at the focal plane of the FMA consisted of a parallel grid avalanche counter (PGAC) filled with isobutane at a pressure of about 3 torr, backed by a 40 × 40 double-sided silicon strip detector (DSSD) with a strip width of 1 mm. The A/q information was obtained from the horizontal (x) position at the PGAC. The energies of the implanted recoils and the subsequent α-decay energies and decay times were provided by the DSSD. A measurement of the time-of-flight between the PGAC and the DSSD, which were ∼40 cm apart, was used to separate ERs from the scattered beam. Around the DSSD, two high-purity germanium (HPGe) clover detectors and two low-energy photon spectrometers (LEPSs) were placed in close geometry to measure γ decays. The data acquisition system was triggered by any DSSD signal above threshold (∼30 keV). A 10 MHz clock provided each event with a time stamp.

Coincident PGAC and DSSD signals were associated with ERs or scattered beam implanted in the DSSD. The energy deposited by ERs was measured with charge-to-digital converters. A DSSD signal without a coincident PGAC pulse defined a decay of an implanted nucleus. The decay signals of the DSSD were routed into shaping amplifiers with three different gains. Those with a full-scale energy of ∼4 MeV were used to record internal conversion electrons; those with a full-scale energy of ∼20 MeV recorded α decays; and delay-line amplifiers with a full energy scale of ∼160 MeV served to measure fission-like events.

B. Calibration

The reaction ^{170}Er(^{50}Ti, xn)$^{220-x}$Th was used to set up and calibrate the detection systems, as well as to calibrate the mass-to-charge information obtained by the FMA. The ERs produced in the setup reaction were identified through the half-lives and energies of their associated α decays. Subsequently, the ERs were identified in mass A and charge q, and the relation between A/q and the horizontal (x) position of ERs passing through the PGAC was derived. This calibration can be found in Fig. 1.

The shaping amplifiers used for the DSSD signals required individual calibrations according to their specific energy ranges. The amplifiers for the medium range (0–20 MeV) were calibrated in two steps. First, an external ^{240}Pu-^{244}Cm source was used to align the energy signals of all the DSSD strips. Then, the known energy of the α lines in the $^{220-x}$Th nuclei from the setup reaction were used to calibrate the composite of all strips. This procedure was necessary because the statistics in the strips from the setup reaction was not

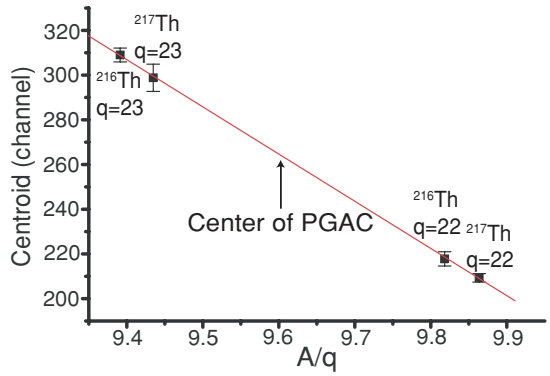

FIG. 1. (Color online) A/q calibration of the FMA PGAC using data from the setup reaction ^{170}Er(^{50}Ti, xn)$^{220-x}$Th. The center of the counter is indicated.

sufficient to calibrate all strips individually. This method also avoided inaccuracies associated with α particles from an external source, which suffer from energy straggling in the dead layer of the DSSD. The energy released in α decay is, due to momentum conservation, shared between the α particle and the recoiling nucleus. Therefore, a part of the detector signal originates from the energy loss of the recoiling daughter nucleus. A calibration based on the known α-decay energies of implanted ERs takes this into account (see, e.g., Ref. [22]). The amplifiers sensitive to the two other energy ranges were calibrated relative to the medium-gain ones by using signals generated by a calibrated precision pulser.

Alpha particles emitted from ERs implanted inside the DSSD can escape and deposit only a fraction of their full energy in the detector, thereby reducing its detection efficiency. The efficiency for full-energy α particles was determined to be $49\% \pm 3\%$ at $\sim$8 MeV. This was measured with data from the setup reaction by comparing the number of counts for first-generation α decays with that of time- and position-correlated second-generation α decays.

The calibration of the germanium detectors was carried out with a number of multiple-line sources. The efficiency was determined for individual detectors, and a total efficiency was obtained from the sum of the individual contributions.

III. RESULTS

A. Mass of the evaporation residues

As stated above, the mass-to-charge-state separation of the FMA was calibrated using data from the setup reaction (see Fig. 1). A PGAC position spectrum for the latter reaction is given in Fig. 2(a). Neighboring masses are separated by eight channels. The horizontal position of ERs produced in the reaction ^{208}Pb(^{50}Ti, n)^{257}Rf is presented in Fig. 2(b). This spectrum was incremented by requiring implant-α correlations. The spectrum establishes that only ERs with mass $A = 257$ were correlated with α decays and contributed to the measured α-decay spectrum of Fig. 3. Note that ^{256}Rf has an α-decay branching ratio of only $b_\alpha = 0.0032 \pm 0.0017$ [17].

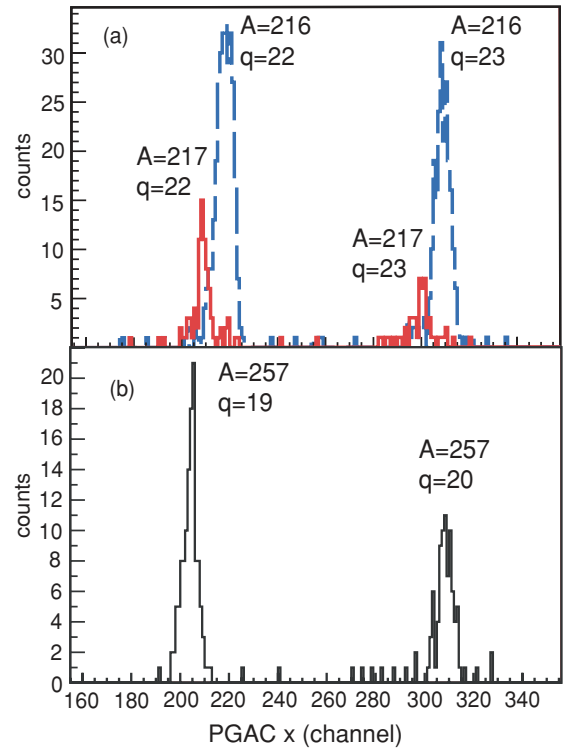

FIG. 2. (Color online) (a) A/q distribution for the ^{170}Er(^{50}Ti, xn)$^{220-x}$Th reaction: the solid (red) line corresponds to $A = 217$ residues and the dashed (blue) line corresponds to $A = 216$, as determined by gating on different α groups. The distance between the neighboring masses is eight channels. (b) A/q distribution for the ^{208}Pb(^{50}Ti, n)^{257}Rf reaction: the center of the spectrum matches that of (a). Based on the A/q calibration shown in Fig. 1, the two peaks shown in the spectrum correspond to $A = 257$. In addition, the distance between neighboring masses is eight channels, and thus only one mass is present.

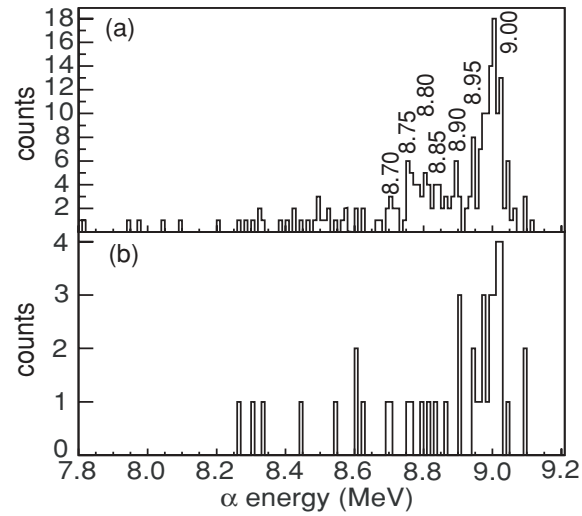

FIG. 3. (a) α-decay energies from evaporation residues (first generation). The centroids of the α transitions are indicated in MeV. (b) First-generation α-decay energies for those events found to be correlated with full-energy second-generation α decays.

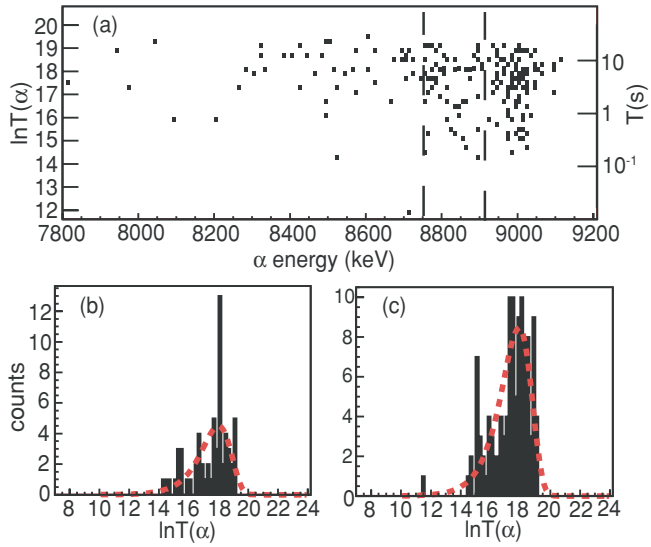

FIG. 4. (Color online) (a) Decay times of first-generation α decay vs α energy for ^{257}Rf. The abscissa is the energy of the first-generation α decay and the ordinate is the corresponding decay time (T is given in units of 100 ns) on a logarithmic scale. A time scale with a logarithm of base 10 is given for comparison on the right-hand side. See text for details. (b) Fit of events in the 8.75–8.91 MeV energy range, resulting in a half-life of $4.4^{+0.6}_{-0.5}$ s. (c) Fit of events in the 8.91–9.20 MeV energy range, resulting in a half-life of $4.1^{+0.4}_{-0.4}$ s.

B. α-decay spectrum

A total of 213 first-generation α decays with $E_\alpha = 8.2$–9.2 MeV were observed in this work (see Fig. 3). Centroids of α lines at 8.7, 8.75, 8.8, 8.85, 8.9, 8.95, and 9.0 MeV are given in the figure. The lack of statistics, together with the summing of the energy signals from α decay and from conversion electron decay, prevent proper determination of the α energy. The associated errors are estimated to be around 0.1 MeV, and do not reflect the intrinsic detector resolution of about 40 keV. All α transitions have similar half-lives [see Fig. 4(a)]. Although low statistics and similar half-lives do not allow for a discussion of individual α lines, the two dominant groups observed in an earlier work by Heßberger *et al.* [17] can clearly be seen in Fig. 3: one is in the 8.75–8.91 MeV energy range and has an associated half-life of $4.4^{+0.6}_{-0.5}$ s [Fig. 4(b)]; the other is in the 8.91–9.2 MeV energy range with a half-life of $4.1^{+0.4}_{-0.4}$ s [Fig. 4(c)].

For second-generation α decays in the 7.8–8.2 MeV energy range, 92 events with a half-life of $1.57^{+0.18}_{-0.15}$ min were observed. Among these, 44 events were correlated with first-generation ^{257}Rf α decays which deposited their full energy in the DSSD. The half-life of these events agrees with the value given in Ref. [17] for ^{253}No α decay. The information on the two generations of α decay is summarized in Table I.

C. Spontaneous fission of ^{257,256}Rf

The energy spectrum associated with high-energy decay events measured in the DSSD is shown in Fig. 5. For these decay events, a time-position correlation with a previously implanted evaporation residue was required. Two groups can be identified: one with energies around 50 MeV and a majority of events located at higher energies. The former group represents random events, based on their very long decay times which exceed the mean time between two subsequent implant events in the same DSSD pixel. The latter group (at higher energies) is consistent with spontaneous fission (SF) events. Saturation of the preamplifier signals accounts for the fact that the SF energies are significantly lower than previously reported values for Rf isotopes [23]. The time-position correlation of the SF events is provided in the lower part of Fig. 6. This spectrum shows only events with an energy of ~120 MeV. Three separate groups can be clearly distinguished. The first one (labeled I in the figure), with 11 counts, is characterized by a half-life of $4.9^{+2.0}_{-1.3}$ ms, which matches that of ^{256}Rf (6.2 ± 0.2 ms [17]). The centroids of events associated with this group in the PGAC position spectrum correspond to $A = 256$ recoils. A second group (II), with 10 counts, has a half-life of $3.2^{+1.4}_{-0.9}$ s, which agrees with the measured α-decay half-life of ^{257}Rf. The position centroid of this group matches, within statistical uncertainty, the centroid of $A = 257$ ERs [see Fig. 6(a)]. The third group (III) is due to randomly time-correlated events:

TABLE I. Summary of α-decay data observed in the present work. The two dominant groups observable in the first-generation α decay are given as $\alpha 1$ and $\alpha 2$; Σ_α: number of first-generation α-decay events; $\Sigma_{\alpha-\alpha}$: number of first-generation, full-energy α-decay events correlated with second-generation, full-energy α decays.

Group	E_α range (MeV)	Σ_α	$T_{1/2}$	$\Sigma_{\alpha-\alpha}$
1st gen. total	8.20–9.20	213	4.7(3) s	44
$\alpha 1$	8.75–8.91	61	$4.4^{+0.6}_{-0.5}$ s	9
$\alpha 2$	8.91–9.20	115	$4.1^{+0.4}_{-0.4}$ s	28
2nd gen. total	7.80–8.20	92	$1.57^{+0.18}_{-0.15}$ min	

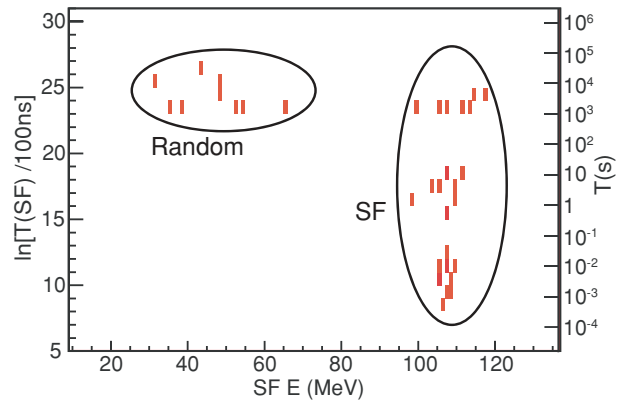

FIG. 5. (Color online) Spontaneous fission events observed in this work. The decay time (in units of 100 ns) is presented on a logarithmic scale as a function of the energy deposited in the DSSD. The spontaneous fission energy is inaccurate because of saturation of preamplifier signals. See text for a discussion of the two labeled groups.

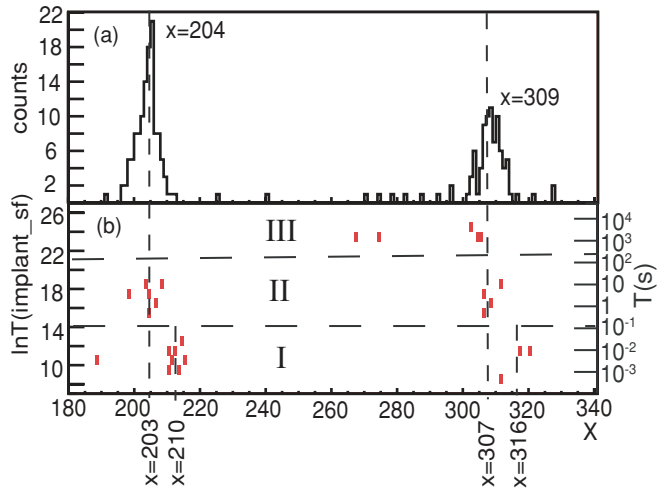

FIG. 6. (Color online) (a) The PGAC horizontal position spectrum of first-generation α particles with energies between 8.2 and 9.2 MeV. (b) The correlation between A/q (obtained from the horizontal position spectrum of the PGAC) and decay times of the SF events in Fig. 5. The abscissa is the PGAC horizontal position. The ordinate is the decay time (in unit of 100 ns) of SF events on a logarithmic scale. A time scale with a logarithm of base 10 is also given on the right-hand side. The horizontal dashed lines separate the SF events into three groups (I–III). The vertical dashed lines indicate their PGAC position centroids. Group II with a half-life of $3.2^{+1.4}_{-0.9}$ s has the same PGAC position centroid, associated with $A = 257$, as the α particles in the upper part of the figure. Group I with a half-life of $4.9^{+2.0}_{-1.3}$ ms has a larger PGAC position centroid, consistent with $A = 256$. Group III, with a much longer half-life, originates from randomly correlated events.

they do not exhibit a localized position correlation [Fig. 6(b)] and likely originate from scattered beam.

D. Conversion electrons

The internal conversion electrons (ICEs) observed in this work are presented in Fig. 7(a). They can be distinguished from α decays by inspecting ICE-α correlations. The ICE energies are expected to be lower than at least the majority of α events which do not deposit their full energy in the DSSD. The information on the ICEs observed in this work is summarized in Table II. In the μs time range, 39 ICE events, which were followed by first-generation α decays, were observed. Of those events, 22 have energies between 8.75 and 9.2 MeV [see Fig. 7(b)] of ^{257}Rf α decays. Eight of those 22 events are followed by second-generation α decays (ER-ICE-α-α correlation), and four of those were succeeded by full-energy ^{253}No α decays. This number is comparable to the five events that would be expected, taking into account the estimated DSSD efficiency and the electron-capture (EC) branch of ^{253}No obtained in this work (see Sec. IV A). These data unambiguously indicate that an isomeric state is present in ^{257}Rf, and we label the corresponding ICEs as group A. The measured half-life of group A is 160^{+42}_{-31} μs. In the 8.75–8.91 MeV energy range, the α decays from ^{257}Rf following group A have a half-life of $2.9^{+1.6}_{-0.9}$ s [see Fig. 7(c)]. For α energies between 8.91 and 9.2 MeV, the correlated α decays have a half-life of $4.6^{+1.4}_{-1.0}$ s [Fig. 7(d)].

A second group of 15 ICE events, which were followed by α decay, is labeled group B in Fig. 7. Those events have a half-life of $4.1^{+2.4}_{-1.3}$ s [Fig. 7(a)]. Five of these events have α energies between 8.75 and 8.91 MeV [Fig. 7(b)]. There are no events in the interval of the strongest α lines (8.91–9.2 MeV); see Fig. 7(b). α decays following ICEs from group B have a half-life of $1.5^{+0.5}_{-0.3}$ s. It is important to note that none of the group B events are accompanied by ^{253}No second-generation α decays. Furthermore, no ER-ICE-ICE-α correlation event was observed for either group A or group B.

Seven γ decays with energies between 80 and 300 keV, which occurred within 20 μs of the detection of group A ICEs, were also observed (see Fig. 8). No coincidences between γ rays and events from group B were detected. Among the seven γ decays, two events match the energies of $K_{\alpha 1}$ (134 keV) and $K_{\alpha 2}$ (126 keV) X rays of Rf, respectively [24].

IV. DISCUSSION

A. Decay properties

The α spectrum of ^{257}Rf was first measured by Bemis *et al.* [25,26] and later by Heßberger *et al.* [17,27,28]. In the experiment described in Refs. [25,26], ^{257}Rf was not implanted inside a silicon detector, but stopped in a He jet and subsequently collected on an aluminum disk that was placed in front of a silicon detector. Rutherfordium was identified by the detection of K X rays from ^{253}No, the α-decay daughter of ^{257}Rf. Summing of the energy signals of α particles and electrons, as discussed in the Introduction, was minimized in the measured α-energy spectrum. In contrast, the corresponding α-decay spectrum from Ref. [17] was obtained,

TABLE II. Summary of the ICE data following ERs and correlated with first-generation α decays; Σ_{ICE}: number of ICE events following ERs; $\Sigma_{\mathrm{ICE}-\alpha}$: number of correlations between ICEs and first-generation α-decay events; $T^{\mathrm{corr}}_{1/2}$: half-life of the ICE-correlated α-decay events. $\alpha 1$ and $\alpha 2$ refer to the two α groups defined in Table I.

Group	Σ_{ICE}	$T_{1/2}$	$\Sigma_{\mathrm{ICE}-\alpha(\alpha 1)}$	$T^{\mathrm{corr}}_{1/2}(\alpha 1)$	$\Sigma_{\mathrm{ICE}-\alpha(\alpha 2)}$	$T^{\mathrm{corr}}_{1/2}(\alpha 2)$
Group A	39	160^{+42}_{-31} μs	7	$2.9^{+1.6}_{-0.9}$ s	15	$4.6^{+1.4}_{-1.0}$ s
Group B	15	$4.1^{+2.4}_{-1.3}$ s	5	$3.5^{+2.4}_{-1.3}$ s[a]	0	–

[a]The half-life for all 15 ICE-correlated α events is $1.5^{+0.5}_{-0.3}$ s.

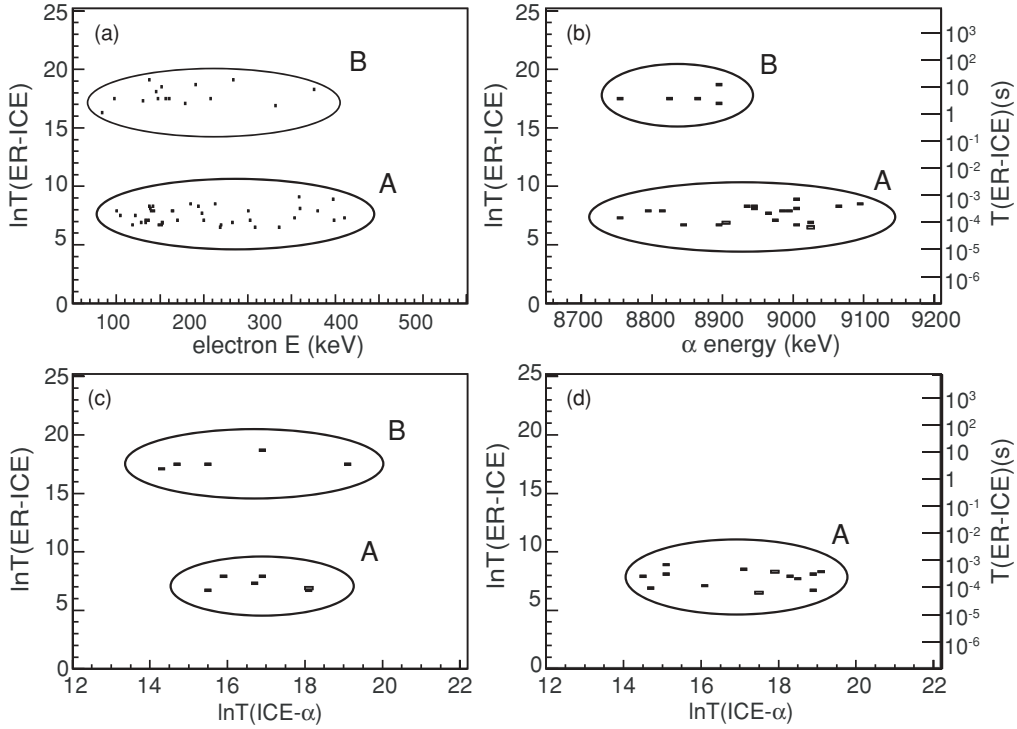

FIG. 7. Lifetime of measured conversion electrons on a log scale as a function of (a) the energy of conversion electrons from ICE-α correlations, (b) the energy of first-generation α decays, (c) the logarithm of the decay time of first-generation α decays gated on energies $E_\alpha = 8.75$–8.91 MeV, and (d) the logarithm of the decay time of ICEs followed by α decays with a gate on $E_\alpha = 8.91$–9.20 MeV. T is the decay time in units of 100 ns. On the right-hand side, time scales with a logarithm of base 10 are given. Two groups are labeled A and B; see text for details.

similar to the present work, by implanting the recoils in a silicon strip detector. As a consequence of the geometry, summing of the α and the electron energy signals can alter the energies and intensities of the observed α lines. Therefore, in proposing a level scheme (see below), we use the intensities from Refs. [25,26] wherever possible; otherwise we utilize the data from Ref. [17]. The data on α decay of ^{257}Rf from this work have lower statistics but are consistent with the earlier results.

The α-decay spectrum of ^{257}Rf is complex. The energies of the α transitions from the ground or low-energy excited states of ^{257}Rf to ^{253}No range from 8.2 to 9.2 MeV. Three dominant

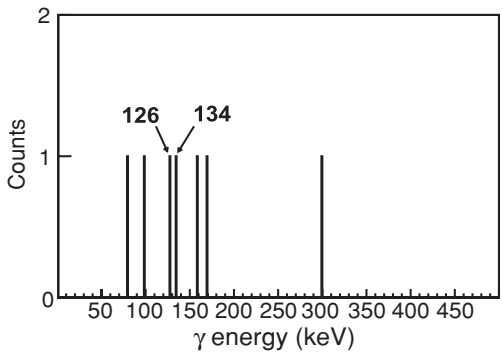

FIG. 8. γ-energy spectrum coincident with the ICE events of group A. $K_{\alpha 1}$ (134 keV) and $K_{\alpha 2}$ (126 keV) X rays of Rf are indicated.

α transitions were reported by both groups [17,25] to have energies of 8778, 8951, and 9016 keV. The corresponding half-lives are 3.5 ± 0.3, 3.6 ± 0.3, and 4.4 ± 0.4 s [17], respectively. In addition, there are many weaker lines. Heßberger *et al.* assigned a total of 12 lines to ^{257}Rf on the basis of 972 counts [17]. Three additional lines were attributed to the α decay of ^{257}Lr, the electron-capture (EC) decay daughter of ^{257}Rf; the dominant line at 8875 keV was reported to have a half-life of $3.3^{+0.5}_{-0.4}$ s [17].

^{257}Rf has been studied with the fusion-evaporation reactions ^{249}Cf(^{12}C, $4n$)^{257}Rf [25,26] and ^{208}Pb(^{50}Ti, n)^{257}Rf (Refs. [17] and this work), as well as via α decay from the reactions ^{208}Pb(^{58}Fe, n)^{265}Hs(α)^{261}Sg(α)^{257}Rf and ^{208}Pb(^{54}Cr, n)^{261}Sg(α)^{257}Rf [28]. A striking result from the latter two reactions is the absence of the strong α lines at 8951 and 9016 keV. The two lines have been interpreted [17] as transitions from an isomeric state which is not populated in ^{261}Sg α decay (see Fig. 9).

The 8778-keV α transition has been shown to populate an isomeric state in ^{253}No, which decays via a delayed 167-keV γ transition to the ground state [28]. As a consequence, we deduce an α energy of 8943 keV for the ground-state to ground-state transition which corresponds to $Q_{\text{g.s.}\to\text{g.s.}} = 9084$ keV. This is in agreement with the highest energy α counts found in third-generation α decay of ^{265}Hs [17]. Assuming that the α line at 9016 keV feeds the ground state of ^{253}No, the deduced Q value implies an isomeric state in ^{257}Rf, with an excitation energy of ~ 75 keV. In Fig. 10, we present these transitions,

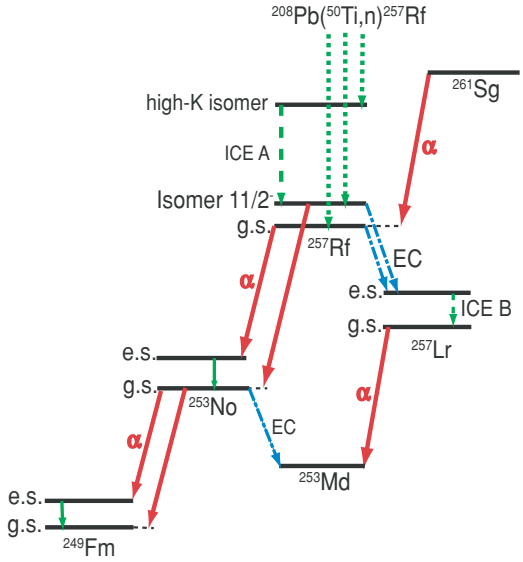

FIG. 9. (Color online) Simplified population and decay scheme of the ground state (g.s.) and isomeric states in ^{257}Rf. The energies of states and transitions are not to scale. Alpha transitions (thick red arrows), electromagnetic transitions (thin green arrows), and electron capture (dash-dotted blue arrows) as well as excited states (e.s.) are indicated schematically. Dotted (green) arrows show the population of states in ^{257}Rf by fusion evaporation. Dashed (green) arrows depict the delayed deexcitation cascades which are the origin of the ICEs observed in this work. The ^{257}Rf ground state has a small EC branch to the ground state of ^{257}Lr, which is not included in this figure for clarity. The α decay from the $11/2^-$ level of ^{257}Rf to excited states of ^{253}No, which cannot be excluded from the available data, as well as spontaneous fission of ^{257}Rf, are also omitted. The figure is based on data from the present work and from Refs. [17,27,28].

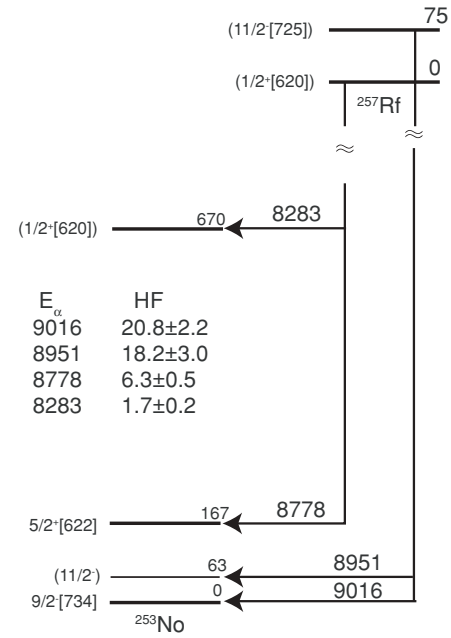

FIG. 10. Partial level and α-decay scheme of ^{257}Rf. The hindrance factors are calculated based on the intensities measured in Refs. [17,26]. The ground-state to ground-state transition ($1/2^+[620] \rightarrow 9/2^-[734]$) is very weak and not shown. Its energy is deduced to be $E_\alpha = 8943$ keV ($Q_\alpha = 9084$) keV. See text for a detailed discussion.

and the assignments discussed below, in a partial level scheme.

In the following, we discuss the Nilsson configurations of the ground and isomeric states of ^{257}Rf based on α-decay hindrance factors. For low-energy states, candidate configurations are $1/2^+[620]$, $3/2^+[622]$, $7/2^+[613]$, $11/2^-[725]$, and $9/2^+[615]$ (see Fig. 11). The hindrance factors given in Fig. 10 have been calculated with the computer program ALPHAD [32] (based on Ref. [33]), following a long-standing procedure used by α spectroscopists. The relatively low hindrance factors of α transitions to the $9/2^-[734]$ and $5/2^+[622]$ states in ^{253}No rule out a spin flip in the transition between the parent and daughter states. Hence, this fact excludes the $3/2^+[622]$ and $9/2^+[615]$ configurations from further consideration as a parent state. The remaining three configurations have distinctly different decay patterns, enabling straightforward assignments for the ground and isomeric states of ^{257}Rf.

Alpha decay from the $1/2^+[620]$ ground states of several $N = 153$ isotones [34–36] strongly populates the $5/2^+[622]$ isomeric state in the daughter. By analogy, we assign the 8778-keV line as this transition, as discussed above. Hence, we assign the ground-state configuration in ^{257}Rf as $1/2^+[620]$. The observed decays support this assignment. The transition to the $9/2^-[734]$ ground state of ^{253}No is highly hindered, as in the other $N = 153$ isotones, due to the large spin change. If the ground-state configuration of ^{257}Rf were $7/2^+[613]$, one would have seen significant decays to both the $5/2^+[622]$ and $9/2^-[734]$ states in the daughter, based on previously observed

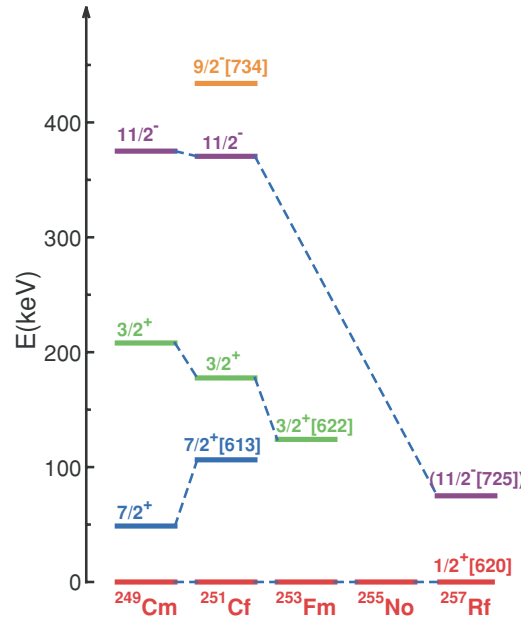

FIG. 11. (Color online) Experimental single-quasiparticle energies for even-Z, $N = 153$ isotones [17,29–31].

hindrance factors for α decays connecting these configurations [37].

In the other known $N = 153$ decays, there is also a strong population of the $1/2^+[620]$ state, which is favored since the initial and final states have the same configuration. In the decay of ^{257}Rf, the only candidate for this transition with the requisite small hindrance factor (1.8) is the weak 8283-keV peak reported in Ref. [17]. This transition has a low intensity because of its low Q value. All the other low-intensity transitions seen by Heßberger *et al.* [17] can be ruled out as a favored transition because of their large hindrance factors.

For the 75-keV isomer in ^{257}Rf, two possible configurations remain from the list given above: $7/2^+[613]$ and $11/2^-[725]$. The observed hindrance factor for the 9016-keV transition favors a $11/2^-[725] \rightarrow 9/2^-[734]$ transition, i.e., to the ground state of ^{253}No. The $7/2^+[613] \rightarrow 9/2^-[734]$ transition is known to be more hindered [37]. The $11/2^-[725]$ assignment is further supported by the relative intensities of the transitions (1:0.73) to the $9/2^-$ and $11/2^-$ rotational band members, which are reasonably close to the estimated values (1:0.5), especially when one considers that Coriolis mixing between the $9/2^-[734]$ and $11/2^-[725]$ configurations would enhance the intensity of the transition to the $11/2^-$ state. Finally, the half-life of the 75-keV isomer supports the proposed configuration assignments for the isomer and the ground state: the large K change between the $11/2^-[725]$ isomer and the $1/2^+[620]$ ground state strongly retards an electromagnetic decay. The long half-life provides a further argument against the $7/2^+[613]$ configuration in either the isomer or the ground state.

A comparison of the decay scheme presented in Fig. 10 and that of Ref. [28] shows both agreements (for the 9016- and 8778-keV assignments) and differences (e.g., energies of $11/2^-$ and $1/2^+$ states). The proposed 63.2-keV energy for the $11/2^-$ state of the $9/2^-[734]$ band, based on the unpublished data of Bemis *et al.* [26], is very close to that observed in other $N = 151$ isotones (^{247}Cm [35], ^{249}Cf [34], ^{251}Fm [38]).

With our proposed energy for the $1/2^+[620]$ state, the trend for $Z = 94$–102 can be inspected for $N = 151$ isotones, as similarly done by Ref. [39]. Figure 12 indicates that the experimental $1/2^+[620]$ quasiparticle energy increases with Z. This energy is important because it reflects the deformed shell gap in the single-particle energies at $N = 152$.

We have calculated the $1/2^+[620]$ quasiparticle energy (with respect to the $9/2^-[734]$ ground state), based on the "universal" Woods-Saxon [43] single-particle energies, with deformation parameters taken from Ref. [44]. Pairing is calculated with the Lipkin-Nogami method [45] and includes blocking. Pairing force strengths of $G_p = 24/A$ and $G_n = 17.8/A$ were used. For the calculations, a truncated configuration space ($N = 5$–7 for neutrons and 4–6 for protons, with N being the number of the major oscillator shell) has been employed. Further details of the model are given in Ref. [46].

Our calculations reproduce the trend of energies due to the variation of the $N = 152$ gap given by the Woods-Saxon potential; see Fig. 12. (Reference [41] gives similar energies, based on calculations with the same potential, but with a different treatment of pairing, using BCS theory, which does not account for blocking.) The theoretical $1/2^+[620]$ energies (with respect to the $9/2^-[734]$ ground state) are given as $E(K = 1/2^+)$, where $E(K)$ is given [47,48] as

$$E(K) = [\varepsilon + R(K)] - \left[\varepsilon_{\text{g.s.}} + R(K_{\text{g.s.}})\right]. \tag{1}$$

In this equation, the calculated one-quasiparticle (1-qp) energy is denoted by ε, while $R(K)$ is given by

$$R(K) = A\{I(I+1) - K^2 + [\langle \mathbf{j}^2 \rangle - \Omega^2] - a\delta_{K1/2}(-1)^{(I+1/2)}(I+1/2)\}. \tag{2}$$

Here A is the rotational parameter, $A = \hbar/(2\mathcal{J})$, with $\mathcal{J}$ being the moment of inertia; K and Ω are the projections on the symmetry axis of the total angular momentum and particle spins, respectively (for a 1-qp state, $K = \Omega$). The value of the decoupling parameter $a = 0.29$ for the $1/2^+[620]$ band is taken from ^{251}Cf. The recoil term $\left[\langle \mathbf{j}^2 \rangle - \Omega^2\right]$ is usually neglected on the grounds that it is part of the single-particle Hamiltonian. However, as argued in Ref. [48], the single-particle energy calculated with a deformed potential (Woods-Saxon in our case) does not include this contribution and, hence, it should be explicitly calculated. Here $\langle \mathbf{j} \rangle$ is calculated based on an expansion of the wave function in terms of the angular momentum $\mathbf{j}$ of the unpaired particle [49]. The net effect is a lowering of $E(1/2^+[620])$ by 169 keV.

The difference between the calculated and experimental $1/2^+[620]$ energies is small at low Z, but increases notably at $Z = 100$ and 102. Hence, the Woods-Saxon single-particle energies are able to reproduce the gap accurately at lower

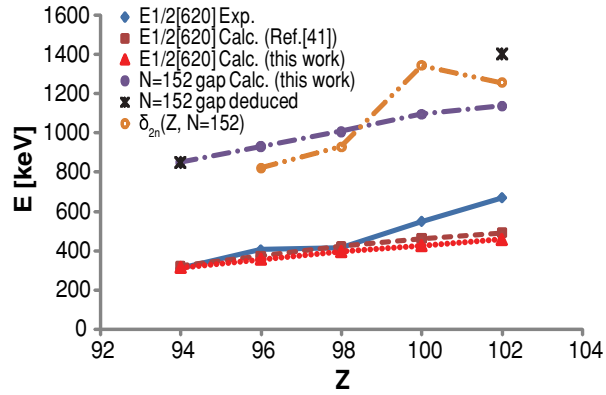

FIG. 12. (Color online) Energy evolution of $1/2^+[620]$ state in $N = 151$ isotones and the size of the shell gap at $N = 152$. The experimental values for the energy of the $1/2^+[620]$ configuration for $Z = 94$–100 are taken from Ref. [40] and for $Z = 102$ from this work (solid blue line). These values are compared with model calculations from this work (dotted line; see text) and from Ref. [41] (dashed line). The results of the model calculations include a correction for the recoil term (see text). For comparison, the size of the single-particle energy gap at $N = 152$, i.e., the energy gap between the $1/2^+[620]$ and the $9/2^-[734]$ configurations, calculated with the Woods-Saxon potential used in this work, is presented (dash-dotted line). Empirical gaps (stars) of 850 and 1400 keV at $Z = 94$ and 102, respectively, would reproduce the measured 1-qp energies. The evolution of the shell gap at $N = 152$ as a function of charge is also reflected in $\delta_{2n}(Z, N)$, the difference of two-neutron separation energies (from Ref. [42]; see dashed doubly-dotted line).

Z, but underestimate it for $Z \geqslant 100$. An increased empirical gap of 1400 keV would reproduce $E(1/2^+[620])$ at $Z = 102$. This represents a sizeable increase from the 850-keV gap at $Z = 94$. The $N = 152$ gap is also reflected in the difference in two-neutron separation energies, $\delta_{2n}(Z, N) = S_{2n}(Z, N) - S_{2n}(Z, N + 2)$, which peaks at $N = 152$ [8]. The variation of $\delta_{2n}(Z, N = 152)$ with Z correlates with the growth of the $N = 152$ gap, as seen in Fig. 12. The cause of the increase of the $N = 152$ shell gap is not understood at this time and constitutes a challenge for theory to describe.

In Ref. [17], it was pointed out that the α-decay half-lives of ^{257}Rf, from population via the reaction ^{208}Pb(^{50}Ti, n)^{257}Rf, were about a factor of 2 shorter than the corresponding half-lives reported from experiments using the ^{208}Pb(^{58}Fe, n)^{265}Hs(α)^{261}Sg(α)^{257}Rf reaction. This work confirms half-lives reported in Ref. [17] from the former reaction. The authors of Ref. [17] speculated about the influence of possible random correlations with scattered beam particles to account for the noted differences in lifetimes. In this work, the higher segmentation of the DSSD, the large A/q dispersion, and the lower beam intensities made longer correlation times (>20 min) possible. Hence, the influence of random correlations on the measured half-lives can be excluded. Contributions from ^{256}Lr, populated in the pn deexcitation channel, can also be ruled out using the A/q information available in the present data set. The origin of the reported discrepancy in the half-lives measured with the two different population mechanisms remains unclear.

The A/q information is important in the investigation of the SF branch of ^{257}Rf, which has in the past been difficult to disentangle from SF of ^{256}Rf [17]. The 10 fission decays observed in the present work yield a SF branching ratio in ^{257}Rf of $b_{\mathrm{Rf}}^{\mathrm{SF}} = 0.02 \pm 0.01$, assuming a detection efficiency for SF events of 100%. This value agrees with the upper limit given in Ref. [17], and is lower than the value reported by Somerville *et al.* [50]. The corresponding ^{257}Rf SF partial half-life is estimated to be 160^{+110}_{-90} s. A comparison of this value with SF partial half-lives of neighboring even-even Rf isotopes [51] indicates a fission hindrance of 10^4–10^5, due to the unpaired neutron.

In this work, the ratio of the time- and position-correlated full-energy α decays between the first two decay generations is 21%; i.e., a smaller value than the 49% DSSD efficiency derived from the setup reaction. This difference arises because (i) the ^{257}Rf ground state has an EC branch, leading to ^{257}Lr, whose α-decay daughter ^{253}Md does not decay by α emission [52], and (ii) ^{253}No, the α-decay daughter of ^{257}Rf, also has an EC branch (see Fig. 9). With $b_{\mathrm{Rf}}^{\mathrm{EC}}$ being the EC-capture branching ratio of ^{257}Rf and $b_{\mathrm{No}}^{\mathrm{EC}}$ that of ^{253}No, the following relation is obtained: $(1 - b_{\mathrm{Rf}}^{\mathrm{EC}})(1 - b_{\mathrm{No}}^{\mathrm{EC}}) = 0.42 \pm 0.07$. (Here, the measured 21% ratio is corrected for the DSSD efficiency.) In Ref. [17], $b_{\mathrm{Rf}}^{\mathrm{EC}}$ was estimated to be $11\% \pm 1\%$, which gives $b_{\mathrm{No}}^{\mathrm{EC}} = 53\% \pm 8\%$, in agreement with a value of $48\% \pm 6\%$ reported in Ref. [53].

B. Model calculations of three-quasiparticle configurations

The information about ^{257}Rf levels available from this and earlier work is such that guidance from model calculations is required to interpret the observations, in particular those related to the isomeric states. These are expected to be associated with 1- or 3-qp configurations. The most likely decay path of isomeric states is expected to proceed to levels of rotational bands via interband transitions. The relative energies of the individual states in these rotational bands govern the decay paths, half-lives, and configurations of high-K isomers.

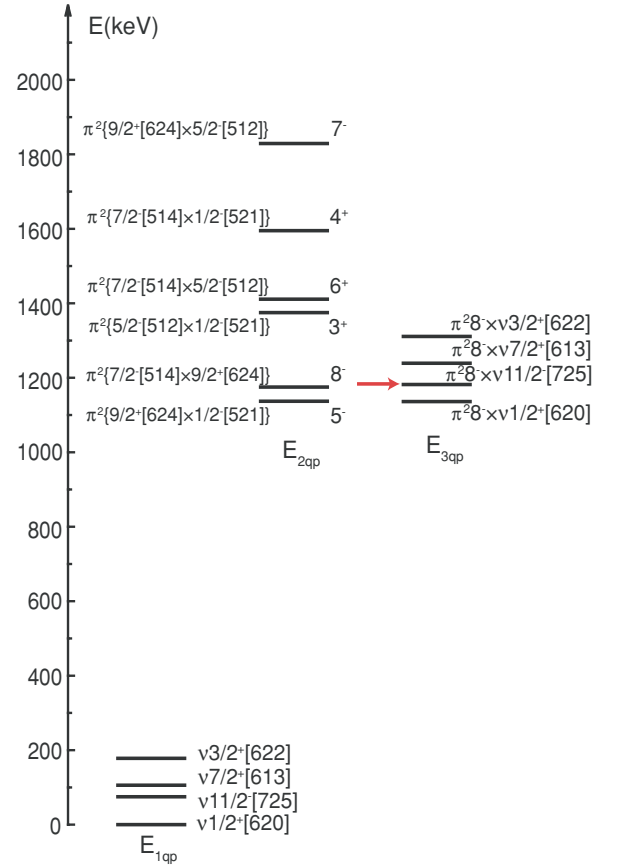

FIG. 13. (Color online) Left column: estimated excitation energies of 1-qp configurations in ^{257}Rf, using the energies measured in ^{251}Cf [29], with the exception of that for the $11/2^-$ state, which is deduced from α decay of ^{257}Rf. Middle column: predicted 2-qp excitation energies obtained from calculations with a Woods-Saxon potential [43] and the Lipkin-Nogami [45] prescription for pairing. Contributions from rotational energy as well as residual spin-spin interaction were taken into account. Right column: excitation energies of 3-qp configurations. A likely configuration for a 160-μs isomer is indicated. See text for details.

In this work, the excitation energies of 1-qp configurations, $E_{1\mathrm{qp}}$, are approximated by taking experimental values from the $N = 153$ isotone ^{251}Cf [29], except for the $11/2^-[725]$ state, which was discussed above (Fig. 13, left column).

The excitation energies of 3-qp states ($E_{3\mathrm{qp}}$) are, to first approximation, given as the sum of the energies of a 2-qp excitation and the odd neutron qp:

$$E_{3\mathrm{qp}}(K) = \varepsilon_{2\mathrm{qp}} + \varepsilon_{\nu 1} - \varepsilon_{\mathrm{g.s.}}. \tag{3}$$

As in Eq. (1), it is necessary to add corrections for the rotational and recoil terms. In addition, residual interactions need to be

accounted for in multi-qp states. Thus,

$$E_{3qp}(K) = [\varepsilon_{2qp} + V_{res}(2qp)] + \varepsilon_{\nu 1} + R(K) + V_{res}(3qp) - [\varepsilon_{g.s.} + R(K_{g.s.})] \quad (4)$$

with

$$R(K) = A[I(I+1) - K^2 + \mathrm{Rec}(K)]. \quad (5)$$

The recoil term $\mathrm{Rec}(K)$ can be shown to be given as the sum of the recoil terms of the individual constituents, i.e.,

$$\mathrm{Rec}(K) = \sum_i [\langle j_i^2 \rangle - \Omega_i^2]. \quad (6)$$

For $T = 1$, 2-qp states, the residual interaction is taken as $V_{res} = -100$ and $+100$ keV for singlet and triplet states (see Ref. [54]). Empirically it is known that there is additional binding from residual interactions $V_{res}(3qp)$ between the odd neutron and the constituents in the 2-qp state. Based on the values found in the Hf region and reducing it due to the larger mass of ^{257}Rf, we make the approximation $V_{res}(3qp) = -100$ keV.

The energies ε_{2qp} of possible 2-qp configurations were obtained from self-consistent multiquasiparticle calculations based on the universal parametrization of the Woods-Saxon potential [43], as discussed in the previous section. The calculation predicts that the lowest 2-qp configurations have a proton-proton character since neutron excitations have to bridge the $N = 152$ gap. The center column of Fig. 13 presents the spectrum of 2-qp excitation energies in ^{257}Rf. In the following, we focus on the 8^-, 2-qp proton configuration, whose high K value and low excitation energy suggests that it is most likely to contribute to a 3-qp isomeric state that is strongly populated.

The estimated excitation energies of 3-qp configurations in ^{257}Rf are presented in the right column of Fig. 13. The rotational parameter A depends on deformation, but since the change in deformation from ^{251}Cf to ^{257}Rf is predicted to be less than 2% [41], the values for 1-qp states from ^{251}Cf serve as approximate values for ^{257}Rf: $A = 6.6$ and 5.3 for 1-qp and 3-qp bands, respectively. However, it is known that for rotational bands built on states containing the high-j, $11/2^-[725]$ configuration smaller values are observed and, we adopt $A = 5.5$ and 4.8 for 1-qp bands and 3-qp bands in this case. The calculated rotational bands are displayed in Fig. 14.

The half-lives of high-K isomers depend on the differences in transition energies to potential daughter states and on the K forbiddeness, quantified by the factor $f_\nu = [(t_{1/2})_{exp}/(t_{1/2})_{WU}]^{1/\nu}$, where $(t_{1/2})_{exp}$ and $(t_{1/2})_{WU}$ are the experimental half-life and the half-life obtained from a Weisskopf estimate [55], respectively; $\nu = (\Delta K - \lambda)$ is the degree of forbiddeness, and λ is the transition multipolarity.

The proposed $11/2^-[725]$ assignment (see Sec. IV A) and the suggested 75-keV excitation energy can be used to test the results of our model calculations. The following test focuses on the $7/2^+[613]$ and $11/2^-[725]$ states as candidates for the configuration of the 75-keV isomer. Note that the members of the rotational band built on this long-lived level are yrast states (see Fig. 14); thus, this band is likely to have a higher population than the ground-state band in a fusion-evaporation

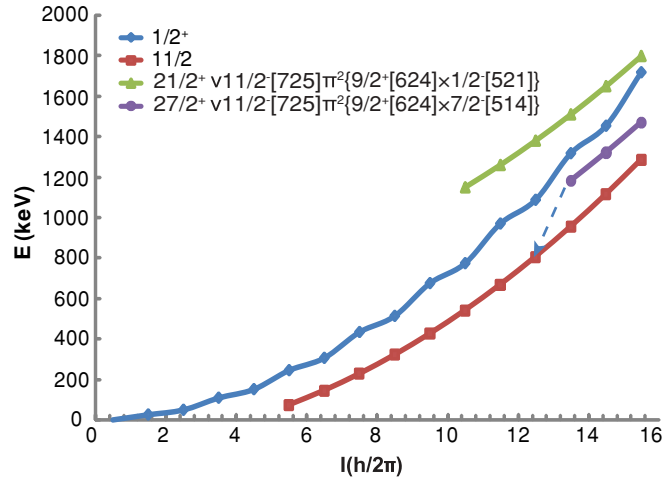

FIG. 14. (Color online) Estimated energies of the rotational bands built on 1-qp and 3-qp bandheads in ^{257}Rf (see text). The dashed blue line indicates a likely decay path from the isomeric state associated with ICE group A. See text for details.

reaction. This is consistent with the observed α spectrum, which exhibits a higher intensity for the high-energy α group.

The $3/2^+$ and $5/2^+$ states of the $1/2^+[620]$ ground-state rotational band are estimated to have energies of ~25 and ~50 keV, respectively. A $7/2^+[613]$ isomeric state at ~75 keV would then decay via a ~25-keV $M1$ transition to this $5/2^+$ level or via a ~50 keV $E2$ transition to the $3/2^+$ level. Using Weisskopf estimates, internal conversion coefficients (ICC) [56,57], and assuming a K forbiddeness of $f_\nu = 10$–100, the calculated half-life associated with the $M1$ transition is 6–600 ns, while the half-life for the $E2$ transition is 2–200 μs. Both calculated half-lives are too short with respect to the measured value of $T_{1/2} \sim 4$ s [17]. The short 37-ns half-life for the decay of the $7/2^+[613]$ state in the $N = 153$ isotone ^{251}Cf also precludes a $7/2^+[613]$ assignment in ^{257}Rf for the 75-keV state. However, if the isomeric state is characterized by a $11/2^-[725]$ configuration, a $11/2^- \rightarrow 5/2^+$, 25-keV $E3$ transition would have an estimated partial half-life of 3–300 s. This encompasses the measured half-life and makes the $11/2^-$ configuration assignment plausible for the isomer-in agreement with the assignment made from α hindrance factors.

C. Interpretation of ICE group A

The observation of ER-ICE-α-α correlations for ICE group A firmly establishes the presence of an isomeric state with a half-life of 160^{+42}_{-31} μs in ^{257}Rf. This level has not been reported before. However, recently Jeppesen *et al.* [58] mentioned an isomeric state in ^{257}Rf with a half-life of 109(13) μs, which agrees within errors with the isomer reported here. No additional information was given in that reference. The α particles correlated with ICE group A include ^{257}Rf lines with energies higher than 8.92 MeV [Fig. 7(b)], indicating a decay path that populates the $11/2^-[725]$ isomer discussed in the previous subsection (see also Fig. 9).

Based on the calculations of Sec. IV B, it is proposed that the measured conversion electrons of group A are associated

with the decay of a 3-qp, high-K isomeric state toward levels belonging to rotational bands built on 1-qp states. The configurations associated with the 3- and 1-qp states would be expected to share the same configuration for the odd neutron, and the transition would involve a 2-qp→0-qp change. The observation of α lines associated with the decay of the $11/2^-[725]$ isomer motivates the choice of this configuration for the odd-neutron component of the 3-qp isomer.

Generally speaking, high-K isomeric states are expected to be located fairly close to the yrast line. Otherwise, a fast decay to lower lying, high-K excited levels could occur. For reasons discussed in Sec. IV B, the $8^-\{\pi 9/2^+[624] \otimes \pi 7/2^-[514]\}$ 2-qp configuration coupled to a 1-qp neutron configuration is the likely origin of a high-K 3-pq configuration. Therefore, the 160-μs isomer is proposed to have a $27/2^+\{8^- \otimes \nu 11/2^-[725]\}$ configuration. This state would decay toward the $25/2^-$ level of the rotational band built on the $11/2^-[725]$ 1-qp level. According to our model calculations, the $25/2^-$ level of the $11/2^-$ band would be located at ∼800 keV and be linked to the $27/2^+$ isomer by a ∼330-keV $E1$ transition. To account for the uncertainty in the transition energy, values between 100 and 500 keV were assumed, resulting in a f_ν factor between 20 and 38. Note that these values are unusually low for an $E1$ transition.

For a K-forbidden $E1$ decay in this mass region, values of $f_\nu \sim 150$–220 are expected, based on isomeric half-lives in some $N = 150$ isotones [59,60] and in ^{254}No [6]. The smaller f_ν value in ^{257}Rf might indicate the onset of a weakening of axial symmetry.

The calculated energies have uncertainties of ∼200 keV. Within this range of uncertainty, it is conceivable that the energy of the $21/2^+\{5^- \otimes \nu 11/2^-[725]\}$ 3-qp level could be lower than that of the $27/2^+$ state. A decrease of $\gtrsim$120 keV in the energy of the former would allow a fast (∼50 ns) decay pathway from the $27/2^+$ bandhead to the band built on the $21/2^+$ configuration. If this were to happen, then the $21/2^+$ state, rather than the $27/2^+$ state, would constitute isomer A.

Figure 7(b) shows seven α events correlated with the ICEs from group A with energies between 8.75 and 8.91 MeV. The α transitions with energies below 8.91 MeV were not associated with the decay of the $11/2^-[725]$ isomer in previous works [17,28]. There are two plausible explanations for the origin of these seven events. Either they could represent new α transitions from the $11/2^-[725]$ isomer to excited states in ^{253}No or the $11/2^-[725]$ state decays via delayed electromagnetic transitions to the ground state of ^{257}Rf, which would then in turn be the source of α lines with $E_\alpha < 8.9$ MeV (see Fig. 9).

The available data are insufficient to distinguish between these two possibilities. For the former explanation, a change of the principal quantum number makes transitions to most excited states in ^{253}No unfavored, except to the $11/2^-[725]$ state. The seven ICE-correlated α events form 32% of all ICE-correlated α decays; this would imply a significant fraction of decays to the ground state of ^{253}No. Lack of statistics prevents the extraction of reliable hindrance factors. The latter explanation requires consistent half-lives: if the $1/2^+[620]$ ground state were in the decay path of the $11/2^-[725]$ isomer, α decays with energies 8.75–8.91 MeV would be expected to have a considerably larger half-life, corresponding roughly to the sum of the half-lives of the $11/2^-[725]$ isomer and the $1/2^+[620]$ ground state. Both α half-lives have been reported to be ∼4 s [17]. In this work, a half-life of $2.9^{+1.6}_{-0.9}$ s for the seven events has been obtained, which is too small compared to the sum of those two half-lives. Further measurements are necessary to probe this explanation.

As mentioned in Sec. III D, one count each of K_α X rays at 126 and 134 keV were observed in coincidence with group A events (Fig. 8). Based on the suggested decay path of the 160-μs isomer, the rotational model employed in this work can be used to estimate the transition energies and probabilities in the $11/2^-[725]$ band. This results in the probabilities per event for emitting $K_{\alpha 1}$ and $K_{\alpha 2}$ X rays of 0.03 and 0.02, respectively. For a total of 39 events in group A and a detection efficiency of ∼19% at ∼130 keV, the expected number of $K_{\alpha 1}$ and $K_{\alpha 2}$ X rays is 0.2 for both. This is about a factor of 5 lower than observed, but not incompatible with the observations. The estimated number of counts at the X-ray energies from random coincidences is $\sim 7 \times 10^{-3}$, suggesting that the x-ray counts indeed originate from ^{257}Rf.

One of the SF events correlated with an $A = 257$ evaporation residue was preceded by a correlated ICE event. The time difference between the implantation of the ER in the DSSD and the detected ICE was 326 μs, while the time difference between the ICE and SF was 1.1 s. These numbers are consistent with the decay time of the 3-qp isomer and the subsequent fission of ^{257}Rf.

D. Interpretation of ICE group B

ICE group B is characterized by a long half-life ($4.1^{+2.4}_{-1.3}$ s) and by correlations with α particles from 8.75 to 8.9 MeV, with none above 8.9 MeV. No correlated ER-ICE-α-α event and no correlation between events from groups A and B was observed. Due to low statistics, little other information is available for group B.

As shown in Fig. 9, ^{257}Rf can deexcite via α decay to ^{253}No and, subsequently, to ^{249}Fm; this would result in ER-ICE-α-α correlations. An alternative ^{257}Rf decay mode, EC, populates ^{257}Lr. This isotope decays subsequently via α emission to ^{253}Md, which has a measured α-decay branching ratio of only $b_\alpha \approx 0.007$ [61]. Therefore, this second path is consistent with the absence of ER-ICE-α-α correlations for the events of group B. If the decay path were to lead to ^{253}No, it is very unlikely that no ER-ICE-α-α correlations would be detected. The probability for this lack of correlation is estimated to be $\sim 10^{-3}$. Hence, the most likely scenario for the origin of ICE group B is ^{257}Rf EC to excited states in ^{257}Lr, which then subsequently emit the ICEs of group B (Fig. 9). The observed implant-electron decay time would then be dominated by the EC capture half-live of ^{257}Rf. With the EC branch (11%) reported in Ref. [17], the partial half-life is ∼37 s. The partial half-lives for EC of the $1/2^+[620]$ ground state of ^{257}Rf to the possible $1/2^-[521]$ ground state of ^{257}Lr is estimated to be 360 s, where a log ft value of 5.8 is assumed for the $1/2^+[620]$ to $1/2^-[521]$ transition by analogy with values in the neighboring ^{249}Cm and ^{251}Cm nuclei [62]. The large discrepancy between the observed and calculated partial

half-lives implies that 90% of the total intensity is expected to populate excited states in ^{257}Lr. The observed correlated α decays are in an energy range that is in agreement with the three lines assigned to the decay of ^{257}Lr: 8636, 8810, and 8875 keV [17]. However, one aspect of this hypothesis is inconsistent with the data: the half-life of the α decays following ICE group B ($1.5^{+0.5}_{-0.3}$ s) is larger than the α-decay half-life of ^{257}Lr (0.6 ± 0.1 s) [63].

In spite of the interpretation of ICE group B given above, the possibility remains that group B originates from an isomeric state in ^{257}Rf. In that case, the high ICE energies (100–350 keV) would suggest the presence of another high-K, 3-qp configuration with a long half-life.

V. SUMMARY AND CONCLUSIONS

Delayed spectroscopy of ^{257}Rf has been performed. The obtained α-decay energies and decay half-lives agree with previous studies. We propose a partial decay scheme of ^{257}Rf and configuration assignments for the ground and isomeric states in ^{257}Rf, as well as for some prominently populated states in ^{253}No. The assignments, which are based on α hindrance factors, differ in some instances from level sequences proposed earlier [17,28] and restore the similarity with the schemes of the neighboring isotones. The assignment of Nilsson configurations on this basis is used to extract the energy of the $1/2^+[620]$ Nilsson configuration in ^{253}No, which reflects the size of the $N = 152$ shell gap. The energies of the $1/2^+[620]$ state in $N = 151$ isotones increase between $Z = 94$ and 102. We deduce that the $N = 152$ gap grows substantially from 850 keV at $Z = 94$ to 1400 keV at $Z = 102$. This growth is confirmed by the differences in two-neutron separation energies.

Spontaneous fission of ^{257}Rf has been unambiguously identified. The A/q information provided by the Fragment Mass Analyzer, combined with different lifetimes, clearly distinguishes between spontaneous fission events in ^{257}Rf and ^{256}Rf. The ratio of the partial half-lives of these isotopes results in a hindrance factor for spontaneous fission of 10^{-4}–10^{-5}, because of the influence of the unpaired neutron in ^{257}Rf.

A new isomeric state, with a half-life of 160^{+42}_{-31} μs, has been observed for the first time by detecting internal conversion electrons followed by α decay. The presence of this isomer in ^{257}Rf can be attributed to a high-K state. A $K^\pi = 27/2^+\{8^- \otimes \nu 11/2^-[725]\}$ configuration is proposed, based on calculations of 3-qp energies with the universal parametrization of the Woods-Saxon potential. It has not been possible to construct a detailed decay scheme because of insufficient γ-ray data. However, the measured decay time of the isomeric state, together with model calculations, has been used to extract the associated K-forbiddeness factor. The value $f_\nu \sim 20$–38 is rather low for an $E1$ transition in this mass region. While the K quantum number is still valid for nuclei with $Z = 104$, this might possibly indicate the onset of a departure from axial symmetry.

A second group of internal conversion electrons correlated with α decays has been observed as well. The half-life of this group has been measured to be $4.1^{+2.4}_{-1.3}$ s. An unambiguous assignment of these events was not possible on the basis of the available data. Most likely, these electrons originate from the decay of excited states in ^{257}Lr after electron capture on ^{257}Rf. However, the possibility of a second 3-qp isomer in ^{257}Rf cannot be ruled out.

The experimental information on the evolution of nuclear structure at the limits of stability is of interest. For high-Z nuclei, detailed spectroscopy is often limited by vanishing production cross sections. The presence of high-K isomers is important in this context. Their decay and the measured correlations with different groups of α particles can not only help disentangle possible decay pathways, but also provide information on the intrinsic structure of levels involved. For example, in this work, the decay of a three-quasiparticle isomer to the $11/2^-$ α-emitting long-lived state suggested a common $11/2^-[725]$ neutron configuration for both levels, a result derived despite the limited data.

ACKNOWLEDGMENTS

The authors thank the ATLAS operations staff for providing stable high-intensity beams and effective support during the experiment. The help of R. C. Pardo in preparing and performing the experiment is gratefully acknowledged. We acknowledge helpful communication from I. Ragnarsson on the recoil term. This work is supported by the US Department of Energy, Office of Nuclear Physics, under Contract Nos. DE-AC02-06CH11357 and DE-FG02-91ER-40609. One author, A.B. Garnsworthy, acknowledges financial support from Nexia Solutions Limited.

[1] S. Hofmann and G. Münzenberg, Rev. Mod. Phys. **72**, 733 (2000).
[2] Y. T. Oganessian *et al.*, Nature (London) **400**, 242 (1999).
[3] S. G. Nilsson, J. R. Nix, A. Sobiczewski, Z. Szymanski, S. Wycech, C. Gustafson, and P. Möller, Nucl. Phys. **A115**, 545 (1968).
[4] M. Bender, K. Rutz, P.-G. Reinhard, J. A. Maruhn, and W. Greiner, Phys. Rev. C **60**, 034304 (1999).
[5] S. Ćwiok, J. Dobaczewski, P. H. Heenen, P. Magierski, and W. Nazarewicz, Nucl. Phys. **A611**, 211 (1996).
[6] S. K. Tandel *et al.*, Phys. Rev. Lett. **97**, 082502 (2006).
[7] M. Bender, P. Bonche, T. Duguet, and P. H. Heenen, Nucl. Phys. **A723**, 354 (2003).
[8] A. V. Afanasjev, T. L. Khoo, S. Frauendorf, G. A. Lalazissis, and I. Ahmad, Phys. Rev. C **67**, 024309 (2003).
[9] R. R. Chasman, I. Ahmad, A. M. Friedman, and J. R. Erskine, Rev. Mod. Phys. **49**, 833 (1977).
[10] J. Randrup, S. E. Larsson, P. Möller, S. G. Nilsson, K. Pomorski, and A. Sobiczewski, Phys. Rev. C **13**, 229 (1976).
[11] R. E. Brown, J. A. Cizewski, E. R. Flynn, and J. W. Sunier, Phys. Rev. C **20**, 1301 (1979).

[12] S. L. Nelson, K. E. Gregorich, I. Dragojević, M. A. Garcia, J. M. Gates, R. Sudowe, and H. Nitsche, Phys. Rev. Lett. **100**, 022501 (2008).
[13] S. Hofmann, Z. Phys. A **358**, 125 (1997).
[14] D. Peterson *et al.*, Phys. Rev. C **74**, 014316 (2006).
[15] F. P. Heßberger, S. Hofmann, D. Ackermann, P. Cagarda, R. D. Herzberg, I. Kojouharov, P. Kuusiniemi, M. Leino, and R. Mann, Eur. Phys. J. A **22**, 417 (2004).
[16] R. D. Herzberg *et al.*, Nature (London) **442**, 896 (2006).
[17] F. Heßberger *et al.*, Z. Phys. A **359**, 415 (1997).
[18] I. Dragojević, K. E. Gregorich, C. E. Düllmann, M. A. Garcia, J. M. Gates, S. L. Nelson, L. Stavsetra, R. Sudowe, and H. Nitsche, Phys. Rev. C **78**, 024605 (2008).
[19] J. F. Ziegler, Program SRIM, http://www.srim.org/.
[20] J. Greene, A. Heinz, J. Falout, and R. Janssens, Nucl. Instrum. Methods Phys. Res. A **521**, 214 (2004).
[21] C. N. Davids, B. B. Back, K. Bindra, D. J. Henderson, W. Kutschera, T. Lauritsen, Y. Nagame, P. Sugathan, A. V. Ramayya, and W. B. Walters, Nucl. Instrum. Methods Phys. Res. B **70**, 358 (1992).
[22] F. Heßberger, S. Hofmann, D. Ackermann, V. Ninov, M. Leino, S. Saro, A. Andreyev, A. Lavrentev, A. Popeko, and A. Yeremin, Eur. Phys. J. A **8**, 521 (2000).
[23] D. C. Hoffman, Nucl. Phys. **A502**, 21 (1989).
[24] *Table of Isotopes*, 8th ed., edited by R. Firestone and V. Shirley (Wiley, New York, 1996).
[25] C. E. Bemis, R. J. Silva, D. C. Hensley, O. L. Keller, J. R. Tarrant, L. D. Hunt, P. F. Dittner, R. L. Hahn, and C. D. Goodman, Phys. Rev. Lett. **31**, 647 (1973).
[26] C. E. Bemis, J. R. Tarrant, R. J. Silva, L. D. Hunt, D. C. Hensley, P. F. Dittner, O. L. Killer, and R. L. Hahn, Oak Ridge National Laboratory Annual Report, ORNL-4976, 1973, p. 37 (unpublished).
[27] F. P. Heßberger *et al.*, AIP Conf. Proc. **495**, 145 (1999).
[28] B. Štreicher *et al.*, Acta Phys. Pol. **38**, 1561 (2007).
[29] I. Ahmad, J. P. Greene, E. F. Moore, F. G. Kondev, R. R. Chasman, C. E. Porter, and L. K. Felker, Phys. Rev. C **72**, 054308 (2005).
[30] R. W. Hoff, W. F. Davidson, D. D. Warner, H. G. Börner, and T. von Egidy, Phys. Rev. C **25**, 2232 (1982).
[31] M. Asai *et al.*, Phys. Rev. Lett. **95**, 102502 (2005).
[32] ALPHAD program, http://www.nndc.bnl.gov/nndcscr/ensdf_pgm/analysis/alphad/.
[33] M. A. Preston, Phys. Rev. **71**, 865 (1947).
[34] I. Ahmad, A. M. Friedman, R. F. Barnes, R. K. Sjoblom, J. Milsted, and P. R. Fields, Phys. Rev. **164**, 1537 (1967).
[35] I. Ahmad, R. R. Chasman, J. P. Greene, F. G. Kondev, E. F. Moore, E. Browne, C. E. Porter, and L. K. Felker, Phys. Rev. C **68**, 044306 (2003).
[36] F. P. Heßberger *et al.*, Eur. Phys. J. A **29**, 165 (2006).
[37] I. Ahmad, F. T. Porter, M. S. Freedman, R. F. Barnes, R. K. Sjoblom, F. Wagner, J. Milsted, and P. R. Fields, Phys. Rev. C **3**, 390 (1971).
[38] M. Asai, K. Tsukada, H. Haba, A. Toyoshima, T. Ishii, Y. Nagame, I. Nishinaka, T. Ichikawa, Y. Kojima, and K. Sueki, JAEA-Tokai TANDEM Annual Report 2005, JAEA-Review 2006-029, 2006 (unpublished).
[39] H. Makii *et al.*, Phys. Rev. C **76**, 061301(R) (2007).
[40] ENSDF database, http://www.nndc.bnl.gov/ensdf.
[41] A. Parkhomenko and A. Sobiczewski, Acta Phys. Pol. B **36**, 3115 (2005).
[42] A. H. Wapstra, G. Audi, and C. Thibault, Nucl. Phys. **A729**, 129 (2003).
[43] S. Ćwiok, J. Dudek, W. Nazarewicz, J. Skalski, and T. Werner, Comput. Phys. Commun. **46**, 379 (1987).
[44] P. Möller, J. R. Nix, W. D. Myers, and W. J. Swiatecki, At. Data Nucl. Data Tables **59**, 185 (1995).
[45] Y. Nogami, Phys. Rev. **134**, B313 (1964).
[46] F. G. Kondev *et al.*, in *Proceedings of the International Conference on Nuclear Data for Science and Technology, 2007*, p. 61, http://nd2007.edpsciences.org.
[47] S. G. Nilsson and I. Ragnarsson, *Shapes and Shells in Nuclear Structure* (Cambridge University Press, Cambridge, England, 1995).
[48] E. Osnes, J. Rekstad, and O. K. Gjøtterud, Nucl. Phys. **A253**, 45 (1975).
[49] I. Ahmad, R. R. Chasman, A. M. Friedman, and S. W. Yates, Phys. Lett. **B251**, 338 (1990).
[50] L. P. Somerville, M. J. Nurmia, J. M. Nitschke, A. Ghiorso, E. K. Hulet, and R. W. Lougheed, Phys. Rev. C **31**, 1801 (1985).
[51] N. E. Holden and D. C. Hoffman, Pure Appl. Chem. **72**, 1525 (2000).
[52] A. K. Jain, S. Singh, and J. K. Tuli, Nucl. Data Sheets **107**, 2103 (2006).
[53] S. Eeckhaudt, JYFL Research Report No. 8, 2006 (unpublished).
[54] K. Katori, I. Ahmad, and A. M. Friedman, Phys. Rev. C **78**, 014301 (2008).
[55] A. Bohr and B. R. Mottelson, *Nuclear Structure* (Benjamin, Reading, MA, 1975), Vol. 1.
[56] T. Kibédi, T. W. Burrows, M. B. Trzhaskovskaya, P. M. Davidson, and C. W. Nestor Jr., Nucl. Instrum. Methods Phys. Res. A **589**, 202 (2008).
[57] Conversion Coefficient Calculator BRICC v2.2.b, http://www.rsphysse.anu.edu.au/nuclear/bricc/index.php.
[58] H. B. Jeppesen *et al.*, Phys. Rev. C **79**, 031303(R) (2009).
[59] A. P. Robinson *et al.*, Phys. Rev. C **78**, 034308 (2008).
[60] P. T. Greenlees *et al.*, Phys. Rev. C **78**, 021303(R) (2008).
[61] F. P. Heßberger *et al.*, Eur. Phys. J. A **26**, 233 (2005).
[62] R. W. Lougheed, J. F. Wild, E. K. Hulet, R. W. Hoff, and J. H. Landrum, J. Inorg. Nucl. Chem. **40**, 1865 (1978).
[63] K. Eskola, P. Eskola, M. Nurmia, and A. Ghiorso, Phys. Rev. C **4**, 632 (1971).